

Phase Diagram of the Gross-Neveu Model: Exact Results and Condensed Matter Precursors

Oliver Schnetz, Michael Thies and Konrad Urlichs¹
Institut für Theoretische Physik III
Universität Erlangen-Nürnberg, Erlangen, Germany

Abstract

Recently the revised phase diagram of the (large N) Gross-Neveu model in 1+1 dimensions with discrete chiral symmetry has been determined numerically. It features three phases, a massless and a massive Fermi gas and a kink-antikink crystal. Here we investigate the phase diagram by analytical means, mapping the Dirac-Hartree-Fock equation onto the non-relativistic Schrödinger equation with the (single gap) Lamé potential. It is pointed out that mathematically identical phase diagrams appeared in the condensed matter literature some time ago in the context of the Peierls-Fröhlich model and ferromagnetic superconductors.

¹Electronic addresses: thies@theorie3.physik.uni-erlangen.de, konrad@theorie3.physik.uni-erlangen.de

1 Introduction

The Gross-Neveu (GN) model in 1+1 dimensions [1] is probably the simplest interacting fermionic field theory one can write down,

$$\mathcal{L} = \bar{\psi}^{(i)} i\gamma^\mu \partial_\mu \psi^{(i)} + \frac{1}{2}g^2 \left(\bar{\psi}^{(i)} \psi^{(i)} \right)^2 \quad (1)$$

(here, $i = 1 \dots N$ is a flavor index, and the model is defined through the 't Hooft limit $N \rightarrow \infty$, $Ng^2 = \text{const.}$ [2]). Yet, as evidenced by more than 900 citations in the hep-archive to date, this toy model has turned out to be quite valuable for a variety of physics questions (for a recent review and a discussion of subtleties associated with low dimensions, see Ref. [3]). If one solves it via semi-classical methods following the original 1974 paper, a surprising number of phenomena of interest to strong interaction physics unfold. Already in Ref. [1] asymptotic freedom, spontaneous breaking of the discrete chiral symmetry $\psi \rightarrow \gamma_5 \psi$, dynamical fermion mass generation and a scalar $q\bar{q}$ bound state (the σ -meson) were demonstrated. The version with continuous chiral symmetry, the two-dimensional Nambu–Jona-Lasinio model [4] (NJL₂) possesses an additional massless π -meson. Shortly afterwards, massive kink [5] and kink-antikink [6] type baryons were derived analytically in the discrete chiral model, whereas the NJL₂ model features massless baryons [7, 8]. Promptly it was shown that chiral symmetry gets restored at finite temperature in a second order phase transition [9, 10].

In contrast to these early works, it took a rather long and winding road to determine the full phase structure of the GN model at finite chemical potential and temperature. In 1985, the first phase diagram was proposed [11], followed by a number of works elaborating on it (see e.g. [12, 13]). Its prominent features were two phases (massive and massless quarks), separated by a line of first and second order transitions meeting at a tricritical point. In a density-temperature plot, a mixed phase would appear in the region of low density and temperature. It can be pictured as droplets of chirally restored vacuum containing extra quarks, embedded in the symmetry broken vacuum — reminiscent of the MIT bag model [14]. At the first order phase transition, the droplets fill all space [3].

This scenario as well as the underlying phase diagram were believed to hold for both variants of the GN model (with discrete and continuous chiral symmetry) [13]. Only in 2000 it was noticed that the phase diagram was hard to reconcile with the known baryon spectrum. In the case of the NJL₂ model, a thermodynamically more stable solution of the mean field equations turned out to be one where the chiral condensate assumes a helical form, namely a circle in the $(\bar{\psi}\psi, \bar{\psi}i\gamma_5\psi)$ plane superimposed with a uniform translation along the x axis (a “chiral spiral” [15]). Since the winding number is equal to baryon number, one can regard this structure as a caricature of a Skyrme crystal [16], a point of view emphasized in Ref. [15]. This helical order parameter was subsequently confirmed in Ref. [17], the (substantially) modified phase diagram of the NJL₂ model is discussed in Ref. [3].

As the bosonization technique based on the massless boson is unavailable in the GN model with discrete chiral symmetry, it took somewhat longer to construct a satisfactory phase diagram for this model. Following a variational calculation which clearly showed

the existence of a crystal ground state at $T = 0$ and any finite density [18], the full phase diagram was obtained in Ref. [19], based on a numerical solution of the Dirac-Hartree-Fock equations. The main new feature is the appearance of a third phase, a kink-antikink crystal, in addition to the two previously known homogeneous phases. It supersedes the mixed phase in the old phase diagram. All transitions are second order, and the tricritical point gets transmuted into a Lifshitz point characteristic for the transition from an inhomogeneous to a homogeneous ordered phase in condensed matter physics [20]. The mechanism which drives the spontaneous breakdown of translational invariance at finite density was identified as Overhauser effect [21] with gap formation at the Fermi surface. More recently, guided by these results, the analytic form of the self-consistent scalar potential at $T = 0$ has been guessed correctly and the self-consistency of the crystal ground state could be established analytically [22]. Many of the previous numerical results can now be written down in a concise, analytical way. Instrumental for this solution was the fact that by using an appropriate scalar potential expressed in terms of Jacobi elliptic functions, the Dirac-Hartree-Fock equation could be mapped onto a Schrödinger equation with the Lamé potential which was solved analytically long time ago [23].

In the present paper, we extend the work of Ref. [22] to finite temperature. It turns out that the ansatz for the self-consistent potential used in [22] is general enough to encompass the self-consistent potential at any temperature and chemical potential. Apart from the obvious benefit of analytic insight into the phase structure of the GN model, our results have proven helpful in uncovering some striking relationship between the GN model and certain problems in condensed matter physics, notably in the context of superconductivity.

This paper is organized as follows: In Sect. 2, we present our two-parameter ansatz for the scalar potential and the solution of the Hartree-Fock-Dirac equation. In Sect. 3, we minimize the grand canonical potential and show self-consistency at finite temperature and chemical potential. We also discuss how to compute thermodynamic observables. In Sect. 4, we map out the phase boundaries by appropriate series expansions, study the $T = 0$ limit and derive an effective action of Ginzburg-Landau type near the multicritical point. Finally in Sect. 5 we point out the close relationship between the phase diagram of the GN model and quasi-one-dimensional condensed matter problems.

2 Ansatz for the scalar potential and solution of the Dirac-Hartree-Fock equation

We apply the relativistic Hartree-Fock approximation which becomes exact in the large- N limit (see [3] for details). The starting point for our discussion is the Dirac-Hartree-Fock equation,

$$\left(\gamma^5 \frac{1}{i} \frac{\partial}{\partial x} + \gamma^0 S(x) \right) \psi(x) = E \psi(x), \quad (2)$$

with the following choice of γ -matrices,

$$\gamma^0 = -\sigma_1, \quad \gamma^1 = i\sigma_3, \quad \gamma^5 = \gamma^0 \gamma^1 = -\sigma_2. \quad (3)$$

In the Gross-Neveu model with discrete chiral symmetry, $S(x)$ is real. In terms of the upper and lower spinor components ϕ_{\pm} the Dirac equation consists of two coupled equations

$$\mp \left(\frac{\partial}{\partial x} \pm S \right) \phi_{\pm} = E \phi_{\mp} \quad (4)$$

which can be decoupled by squaring,

$$\left(-\frac{\partial^2}{\partial x^2} \mp \frac{\partial S}{\partial x} + S^2 \right) \phi_{\pm} = E^2 \phi_{\pm}. \quad (5)$$

Eqs. (2-5) fall into the pattern of supersymmetric (SUSY) quantum mechanics. As ansatz for S we choose the superpotential of the Lamé potential [24],

$$S(x) = A\kappa^2 \frac{\text{sn}(Ax, \kappa)\text{cn}(Ax, \kappa)}{\text{dn}(Ax, \kappa)}, \quad (6)$$

where sn , $\text{cn} = \sqrt{1 - \text{sn}^2}$, and $\text{dn} = \sqrt{1 - \kappa^2 \text{sn}^2}$ are Jacobi elliptic functions to the modulus κ [25]. We introduce dimensionless variables

$$\xi = Ax, \quad \tilde{S}(\xi) = S(x)/A, \quad \omega = E/A \quad (7)$$

and find that \tilde{S} has period $2\mathbf{K}$, where $\mathbf{K} = \mathbf{K}[\kappa]$ is the complete elliptic integral of the first kind. Moreover the scalar potential satisfies the symmetry condition

$$\tilde{S}(\xi + \mathbf{K}) = -\tilde{S}(\xi). \quad (8)$$

With the ansatz (6), the second order equation (5) becomes

$$\left(-\frac{\partial^2}{\partial \xi^2} + 2\kappa^2 \text{sn}^2(\xi, \kappa) \right) \phi_{\pm}(\xi) = (\omega^2 + \kappa^2) \phi_{\pm}(\xi) \quad (9)$$

the simplest case of the Lamé equation (with a single gap). The solutions are well known [23, 26],

$$\phi_{\pm}(\xi) = \mathcal{N} \frac{\text{H}(\xi + \alpha)}{\Theta(\xi)} e^{-Z(\alpha)\xi} \quad (10)$$

where H , Θ and Z are the Jacobi eta, theta and zeta function, respectively [25]. (Regrettably there exist different conventions for the argument of the Jacobi zeta function. We choose the convention with $Z(\mathbf{K}) = 0$). The parameter α is related to the (reduced) energy ω and Bloch momentum p by

$$|\omega| = \text{dn}(\alpha, \kappa), \quad p = -iZ(\alpha) + \frac{\pi}{2\mathbf{K}}. \quad (11)$$

Note that α and $-\alpha$ supply the two independent solutions for a given energy eigenvalue ω . The condition for real valued energy and momentum leads to two energy bands $\omega^2 = 0 \dots (1 - \kappa^2)$, $p = 0 \dots \pi/2\mathbf{K}$ and $\omega^2 = 1 \dots \infty$, $p = \pi/2\mathbf{K} \dots \infty$. The lower band is parametrized by $\alpha = \mathbf{K} + i(\mathbf{K}' - \eta)$, the upper band by $\alpha = i\eta$, where in both cases

$\eta = 0 \dots \mathbf{K}' \equiv \mathbf{K}[\sqrt{1 - \kappa^2}]$. From Eq. (11) we calculate ($\mathbf{E} = \mathbf{E}[\kappa]$ is the complete elliptic integral of the second kind)

$$\frac{dp}{d\omega} = \pm \frac{\omega^2 - \mathbf{E}/\mathbf{K}}{\sqrt{(\omega^2 - 1 + \kappa^2)(\omega^2 - 1)}}, \quad (12)$$

where the plus sign refers to the upper band, the minus sign to the lower band. We chose the sign of α in such a way that the slope of the dispersion relation is positive in both bands. The eigenfunction corresponding to $-\alpha$ has quasi-momentum $\pi/\mathbf{K} - p$. The full dispersion relation is plotted in Fig. 1.

With ϕ_+ given, ϕ_- follows from the Dirac equation (4),

$$\phi_- = -\frac{1}{\omega} \left(\frac{\partial}{\partial \xi} + \tilde{S} \right) \phi_+. \quad (13)$$

More explicitly, from Eqs. (4) and (8) we can read off that a simultaneous translation $\xi \rightarrow \xi + \mathbf{K}$ and a discrete chiral transformation $\psi \rightarrow \gamma^5 \psi$ leaves the Dirac equation invariant. Thus $\gamma^5 \psi(\xi + \mathbf{K}) \propto \psi(\xi)$, or equivalently $c\phi_+(\xi) = \phi_-(\xi + \mathbf{K})$, $c\phi_-(\xi) = -\phi_+(\xi + \mathbf{K})$ for some constant c . By iteration we find

$$c^2 \phi_+(\xi) = -\phi_+(\xi + 2\mathbf{K}) = -e^{ip2\mathbf{K}} \phi_+(\xi). \quad (14)$$

Comparison with (10) determines c up to a sign ambiguity which can be resolved by an explicit calculation,

$$\phi_-(\xi) = -\text{sgn}(\omega) e^{\mathbf{K}Z(\alpha)} \phi_+(\xi + \mathbf{K}). \quad (15)$$

We still have to determine the normalization factor \mathcal{N} in Eq. (10). In a continuum normalization, the spatially averaged fermion density should be normalized to 1,

$$1 = \langle \psi^\dagger \psi \rangle = \frac{1}{2\mathbf{K}} \int_0^{2\mathbf{K}} d\xi 2|\phi_+|^2. \quad (16)$$

Inserting (10) and using an addition theorem for \mathbf{H} (note that $\mathbf{H}(x+y)\mathbf{H}(x-y)/\Theta^2(x)\Theta^2(y)$ is elliptic in x and y and thus determined up to an additive constant by its pole structure)

$$\frac{\mathbf{H}(x+y)\mathbf{H}(x-y)}{\Theta^2(x)\Theta^2(y)} = \frac{\pi}{2\mathbf{K}\kappa\sqrt{1-\kappa^2}} \left(\text{dn}^2(y, \kappa) - \text{dn}^2(x, \kappa) \right) \quad (17)$$

leads to

$$|\phi_+|^2 = |\mathcal{N}|^2 \frac{\pi\Theta^2(\alpha)}{2\mathbf{K}\kappa\sqrt{1-\kappa^2}} \left| \text{dn}^2(\alpha, \kappa) - \text{dn}^2(\xi, \kappa) \right|. \quad (18)$$

The spatial average is easily computed. We find

$$|\mathcal{N}|^2 = \frac{\mathbf{K}\kappa\sqrt{1-\kappa^2}}{\pi\Theta^2(\alpha)|\text{dn}^2(\alpha, \kappa) - \mathbf{E}/\mathbf{K}|}. \quad (19)$$

With Eq. (11) we can simplify the expression for $|\phi_+|^2$ to

$$|\phi_+|^2 = \frac{1}{2} \frac{\omega^2 - \text{dn}^2(\xi, \kappa)}{\omega^2 - \mathbf{E}/\mathbf{K}}. \quad (20)$$

Let us now calculate $\bar{\psi}\psi$ and $\psi^\dagger\psi$, the scalar and baryon densities for a single orbit. We find

$$\bar{\psi}\psi = -(\phi_+^*\phi_- + \phi_-^*\phi_+) = \frac{1}{\omega}(\partial_\xi + 2\tilde{S})|\phi_+|^2 \quad (21)$$

and with Eq. (20)

$$\bar{\psi}\psi = \frac{\omega}{\omega^2 - \mathbf{E}/\mathbf{K}}\tilde{S}. \quad (22)$$

Notice that every orbit has the ξ -dependence of the Lamé superpotential. On the other hand Eq. (15) implies $\psi^\dagger\psi = |\phi_+(\xi)|^2 + |\phi_+(\xi + \mathbf{K})|^2$. Using Eq. (20) and the addition theorem for $\text{dn}(\xi + \mathbf{K}, \kappa)$ leads to

$$\psi^\dagger\psi = \frac{\omega^2 - 1 + \kappa^2/2 + \tilde{S}^2/2}{\omega^2 - \mathbf{E}/\mathbf{K}}. \quad (23)$$

From the normalization condition $\langle\psi^\dagger\psi\rangle = 1$ we deduce the spatial average

$$s^2 \equiv \langle\tilde{S}^2\rangle = 2 - \kappa^2 - 2\mathbf{E}/\mathbf{K}. \quad (24)$$

This completes the preparations needed for calculating the grand canonical potential density.

3 The grand canonical potential

In order to determine the phase diagram of the GN model, one has to minimize the grand canonical potential in the space of scalar potentials $S(x)$. We will show that the two-parameter ansatz (6) provides a self-consistent solution so that it is sufficient to minimize with respect to A and κ . In the relativistic Hartree-Fock approximation, the grand canonical potential density per flavor is given by (see [3] and references therein)

$$\Psi = -\frac{1}{\beta\pi} \int_0^{\Lambda/2} dq \ln \left[(1 + e^{-\beta(E-\mu)}) (1 + e^{\beta(E+\mu)}) \right] + \frac{1}{2Ng^2\lambda} \int_0^\lambda dx S^2(x), \quad (25)$$

Here, $\Lambda/2$ is the ultra-violet cutoff, $\lambda = 2\mathbf{K}/A$ the spatial period of $S(x)$, and $q = Ap$. We change to ω as integration variable, spelling out the contributions from the two energy bands. With Eqs. (12) and (24) we find

$$\Psi = -\frac{A}{\beta\pi} \left(\int_0^{\sqrt{1-\kappa^2}} d\omega + \int_1^{\Lambda_\omega} d\omega \right) \frac{dp}{d\omega} \ln \left[(1 + e^{-\beta(A\omega-\mu)}) (1 + e^{\beta(A\omega+\mu)}) \right] + \frac{A^2 s^2}{2Ng^2}. \quad (26)$$

From Eq. (11) we extract the behavior of ω for large p and find that $\Lambda_\omega = \omega(q = \Lambda/2) = \Lambda/2A + As^2/\Lambda + \mathcal{O}(\Lambda^{-3})$. Due to the quadratic divergence, we have to keep the $1/\Lambda$ term.

In the following it is convenient to combine the integral over both energy bands as well as over positive and negative energy modes into the real part of a single integral in the complex plane. The path of integration is shifted slightly away from the real axis. We find

that $dp/d\omega$ defines a double cover of the complex plane and choose the sheet by requiring $dp/d\omega > 0$ for $\omega > 1$. The gaps and the sign-change in Eq. (12) match the behavior of $dp/d\omega$ in the complex plane. Setting

$$a = \beta A, \quad \nu = \beta \mu, \quad (27)$$

we obtain

$$\pi\beta^2\Psi = \frac{\pi a^2 s^2}{2Ng^2} - a \lim_{\varepsilon \rightarrow 0} \operatorname{Re} \int_{-\Lambda_\omega + i\varepsilon}^{\infty + i\varepsilon} d\omega \frac{\omega^2 - \mathbf{E}/\mathbf{K}}{\sqrt{(\omega^2 - 1 + \kappa^2)(\omega^2 - 1)}} \ln(1 + e^{-a\omega + \nu}). \quad (28)$$

The physical value of Ψ for given β and μ is determined by the minimum of Ψ in the two-dimensional space $(\kappa, A) \in (0 \dots 1, 0 \dots \infty)$.

It turns out to be convenient to minimize Ψ in the directions given by two specific linear combinations of $\partial/\partial A$ and $\partial/\partial \kappa$, corresponding to $a\partial/\partial a + \mathbf{K}\partial/\partial \mathbf{K}$ and $a\partial/\partial a - s\partial/\partial s$. Consequently we introduce

$$\begin{aligned} F_1 &= \frac{1}{a^2(1 - \mathbf{E}/\mathbf{K})} \left(a \frac{\partial}{\partial a} - \frac{1 - \kappa^2}{1 - \kappa^2 - \mathbf{E}/\mathbf{K}} \kappa \frac{\partial}{\partial \kappa} \right) \pi\beta^2\Psi \quad \text{and} \\ F_2 &= \frac{1 - \kappa^2 - \mathbf{E}/\mathbf{K}}{a^2(1 - \mathbf{E}/\mathbf{K})} \left(a \frac{\partial}{\partial a} - \frac{(2 - \kappa^2 - 2\mathbf{E}/\mathbf{K})(1 - \kappa^2)}{(1 - \kappa^2 - \mathbf{E}/\mathbf{K})^2} \kappa \frac{\partial}{\partial \kappa} \right) \pi\beta^2\Psi \end{aligned} \quad (29)$$

where we have converted $\partial/\partial \mathbf{K}$ and $\partial/\partial s$ into the $\partial/\partial \kappa$ terms. The calculation of F_1 and F_2 is straightforward (replace ω by ω/a in Ψ before differentiation),

$$\begin{aligned} F_1 &= \frac{\pi}{Ng^2} - 1 + \frac{1}{a} \lim_{\varepsilon \rightarrow 0} \operatorname{Re} \int_{-\frac{\Lambda\beta}{2a} + i\varepsilon}^{\infty + i\varepsilon} d\omega \left(\frac{\partial}{\partial \omega} \frac{\omega}{\sqrt{(\omega^2 - 1 + \kappa^2)(\omega^2 - 1)}} \right) \ln(1 + e^{-a\omega + \nu}), \\ F_2 &= \frac{1}{a} \lim_{\varepsilon \rightarrow 0} \operatorname{Re} \int_{-\infty + i\varepsilon}^{\infty + i\varepsilon} d\omega \left(\frac{\partial}{\partial \omega} \frac{(1 - \kappa^2) - \omega^2 \mathbf{E}/\mathbf{K}}{\sqrt{(\omega^2 - 1 + \kappa^2)(\omega^2 - 1)}} \right) \frac{1}{\omega} \ln(1 + e^{-a\omega + \nu}). \end{aligned} \quad (30)$$

Note that the integral in F_1 is logarithmically divergent as $\Lambda \rightarrow \infty$, whereas the integral in F_2 is convergent. Hence F_2 is a function of a, ν, κ only. In the range $0 < \kappa < 1$, $0 < A$, minimizing Ψ is equivalent to $F_1 = F_2 = 0$. This defines the crystal phase. It exists only in a certain region in the (T, μ) -plane (see [19] and Sect. 4). In this region the value of Ψ has to be compared with the (mathematically) co-existing value of Ψ for the massless Fermi gas (corresponding to $\kappa = 0$ or $A = 0$) and the value of Ψ for the massive Fermi gas (corresponding to $\kappa = 1$). It has been checked numerically that the crystal solution (whenever it exists) is thermodynamically most stable. This result is confirmed by an analytical investigation near the phase boundaries as well as at $T = 0$, cf. Sect. 4.

One advantage of our particular choice of direction in which we minimized the potential [cf. Eq. (29)] is the fact that $F_1 = 0$ is equivalent to the self-consistency of our ansatz. To show this we manipulate the thermal expectation value (note the sign change for negative ω in Eq. (22))

$$\langle \bar{\psi}\psi \rangle_{\text{th}} = \frac{1}{\pi} \int_0^{\Lambda/2} dq \bar{\psi}\psi \left(\frac{1}{e^{\beta(E-\mu)} + 1} - \frac{1}{e^{\beta(-E-\mu)} + 1} \right) \quad (31)$$

in the way we reformulated Ψ . With Eqs. (12), (22) we obtain

$$\langle \bar{\psi}\psi \rangle_{\text{th}} = \frac{1}{\pi} S(x) \lim_{\varepsilon \rightarrow 0} \text{Re} \int_{-\frac{\Lambda\beta}{2a} + i\varepsilon}^{\infty + i\varepsilon} d\omega \frac{\omega}{\sqrt{(\omega^2 - 1 + \kappa^2)(\omega^2 - 1)}} \frac{1}{(e^{a\omega - \nu} + 1)}. \quad (32)$$

Applying a partial integration in Eq. (30) we can use F_1 to express $\langle \bar{\psi}\psi \rangle_{\text{th}}$ as follows,

$$\langle \bar{\psi}\psi \rangle_{\text{th}} = \frac{1}{\pi} S(x) \left(F_1 - \frac{\pi}{Ng^2} \right). \quad (33)$$

This in turn reduces to the self-consistency condition $S(x) = -Ng^2 \langle \bar{\psi}\psi \rangle_{\text{th}}$ for $F_1 = 0$.

In order to isolate the divergencies and to make expansions for $k \rightarrow 0$, $k \rightarrow 1$, and $a \rightarrow 0$ easier accessible, we cast Ψ , F_1 , F_2 into a different form. The transformation amounts to changing from the integrals over the two energy bands to an integration over the single gap. Here we simply give the results which can be verified by comparing the Taylor expansions of corresponding functions at $a = 0$. Whereas the results for the transformed expressions are trivial (cf. Eqs. (61), (62)), some work is needed to expand Eqs. (28), (30) at $a = 0$. The calculations are lengthy but straightforward if one proceeds as follows:

1. replace ω by ω/a as integration variable.
2. show that the expansion in $a = 0$ can be derived from expanding the integrand.
3. use integration by parts twice to obtain the factor $[\ln(1 + e^{-\omega + \nu})]'' = \left(2 \cosh \frac{\omega - \nu}{2}\right)^{-2}$. This renders the integrals finite for $\Lambda \rightarrow \infty$.
4. The a^0 - term can be converted into a sum and thus evaluated.
5. Using the residue theorem, the remaining terms can be converted into a sum over Matsubara frequencies (the a^2 term needs some extra attention).
6. The sum over the Matsubara frequencies can be evaluated yielding rational multiples of $\zeta(2k + 1)$ (where ζ is the Riemann zeta function and $k = 1, 2, \dots$).
7. Comparison with the power series of $\text{Im} \ln \Gamma\left(\frac{1}{2} + \frac{i\nu}{2\pi}\right)$ at $a = 0$ allows one to give the result in terms of $\text{Im} \ln \Gamma$ and its derivatives.

Proving the results is now equivalent to deriving Eq. (61).

We reintroduce A and μ to show the dependence on the basic parameters of our ansatz:

$$\begin{aligned} \Psi = & -\frac{\Lambda^2}{8\pi} - \frac{\mu\Lambda}{2\pi} - \frac{\pi}{6\beta^2} - \frac{\mu^2}{2\pi} + \frac{2A^2}{\pi^2} \int_0^{\pi/2} d\varphi \left(\Delta_\varphi^2 - \frac{\mathbf{E}}{\mathbf{K}} \right) \\ & \left[\text{Re} \frac{\pi}{i\beta A \Delta_\varphi} \ln \frac{\Gamma\left(\frac{1}{2} + \frac{i\beta}{2\pi}(\mu + A\Delta_\varphi)\right)}{\Gamma\left(\frac{1}{2} + \frac{i\beta}{2\pi}(\mu - A\Delta_\varphi)\right)} - \ln \frac{\Lambda\beta}{4\pi} + \frac{\pi}{Ng^2} \right] \end{aligned} \quad (34)$$

where

$$\Delta_\varphi = \sqrt{1 - \kappa^2 \sin^2(\varphi)}. \quad (35)$$

The quadratically and linearly divergent terms (energy density $-\Lambda^2/8\pi$ and baryon density $-\mu\Lambda/2\pi$ of the Dirac sea) are irrelevant and can simply be dropped. From now on, we will work in units where the dynamical fermion mass in the vacuum is 1. In these units the vacuum gap equation reads

$$\frac{\pi}{Ng^2} = \ln \Lambda. \quad (36)$$

Invoking this equation, all remaining infinities are removed and we obtain the renormalized expression

$$\pi\beta^2\Psi_{\text{ren}} = -\frac{\pi^2}{6} - \frac{\nu^2}{2} - \frac{a^2s^2}{2} \ln \frac{\beta}{4\pi} + 2a \int_0^{\pi/2} d\varphi \left(\Delta_\varphi - \frac{\mathbf{E}}{\mathbf{K}\Delta_\varphi} \right) \text{Im} \ln \frac{\Gamma\left(\frac{1}{2} + \frac{i}{2\pi}(\nu + a\Delta_\varphi)\right)}{\Gamma\left(\frac{1}{2} + \frac{i}{2\pi}(\nu - a\Delta_\varphi)\right)}. \quad (37)$$

Similarly we obtain ($\psi = (\ln \Gamma)'$)

$$F_{1,\text{ren}} = -\ln \frac{\beta}{4\pi} + \frac{1}{\pi} \int_0^{\pi/2} d\varphi \text{Re} \left[\psi \left(\frac{1}{2} + \frac{i}{2\pi}(\nu + a\Delta_\varphi) \right) + (a \rightarrow -a) \right], \quad (38)$$

$$F_2 = 2a \frac{\partial}{\partial a} \frac{1}{a} \int_0^{\pi/2} d\varphi \left(\frac{1 - \kappa^2}{\Delta_\varphi^3} - \frac{\mathbf{E}}{\mathbf{K}\Delta_\varphi} \right) \text{Im} \ln \frac{\Gamma\left(\frac{1}{2} + \frac{i}{2\pi}(\nu + a\Delta_\varphi)\right)}{\Gamma\left(\frac{1}{2} + \frac{i}{2\pi}(\nu - a\Delta_\varphi)\right)}. \quad (39)$$

We immediately see that $\Psi_{\text{ren}}(\beta, a^2, \nu^2, \kappa^2)$, $F_{1,\text{ren}}(\beta, a^2, \nu^2, \kappa^2)$ and $F_2(a^2, \nu^2, \kappa^2)$ are even, analytical functions in a , ν and κ . A practical procedure to solve $F_{1,\text{ren}} = F_2 = 0$ is as follows:

1. Choose values for two out of the three parameters $a = 0 \dots \infty$, $\nu = 0 \dots \infty$, $\kappa = 0 \dots 1$.
2. Solve $F_2 = 0$ (Eq. (39)) for the third parameter. This requires finding the zeros of a function of one variable given as a one-dimensional integral.
3. Solve (trivially) $F_{1,\text{ren}} = 0$ (Eq. (38)) for β .
4. With $\{A = a/\beta, \mu = \nu/\beta, \kappa, T = 1/\beta\}$ given, the potential density (37) and all observables are given at one point in the crystal phase in the (T, μ) -plane.

Note that the translationally invariant solution is obtained by setting $\kappa = 1$ and skipping step 2.

This enables us to compute the phase diagram and to explore all limits of interest (see Sect. 4). We illustrate the result of the minimization procedure by plotting lines of constant A and κ in the (μ, T) -plane, see Fig. 2. To clarify this diagram, we also show separately the lines $A = \text{const.}$ and $\kappa = \text{const.}$ in Figs. 3 and 4. The thick lines in Fig. 3

correspond to $A = 0$ (phase boundary between massive and massless phases) and $A = 1$. Like a “separatrix” the latter curve divides the plot into regions where the lines $A = \text{const.}$ emanate from the μ -axis (for $A > 1$) and from the T -axis (for $A < 1$), respectively. The other end of the curves lies on the phase boundary between crystal and massless phases. For $A < 1$, the kink visible in the contour lines reflects the phase boundary between crystal and massive phases. In Fig. 4, the thick curves marked $\kappa = 0$ and $\kappa = 1$ correspond to phase boundaries between crystal phase and the two others. We shall return to this phase diagram in Sect. 4.

For later use notice that the potential density at its minimum is equivalent to the simpler expression

$$\begin{aligned} \pi\beta^2\Psi_1 &\equiv \pi\beta^2\Psi_{\text{ren}} - \frac{a^2s^2}{2}F_1 + a^2F_2 \\ &= -\frac{\pi^2}{6} - \frac{\nu^2}{2} - \frac{a^2\kappa^2}{2\pi} \int_0^{\pi/2} d\varphi \cos(2\varphi) \text{Re} \left[\psi \left(\frac{1}{2} + \frac{i}{2\pi}(\nu + a\Delta_\varphi) \right) + (a \rightarrow -a) \right] \end{aligned} \quad (40)$$

The standard thermodynamic observables can be computed in a straightforward manner, once the grand canonical potential density Ψ (see Eq. (37)) is known. The pressure P , the (spatially averaged) baryon density ρ , the entropy density s and the energy density u are given by

$$\begin{aligned} P &= -\Psi, & \rho &= -\frac{\partial}{\partial\mu}\Psi, \\ s &= \beta^2\frac{\partial}{\partial\beta}\Psi, & u &= Ts - P + \mu\rho. \end{aligned} \quad (41)$$

The x -dependence of the baryon density in the crystal demands some extra attention. In analogy to Eqs. (31), (32), we find for $\rho(x) = \langle \psi^\dagger \psi \rangle_{\text{th}}$

$$\begin{aligned} \rho(x) &= \frac{1}{\pi} \int_0^{\Lambda/2} dp \psi^\dagger \psi \left(\frac{1}{e^{\beta(\omega-\mu)} + 1} - \frac{1}{e^{\beta(-\omega-\mu)} + 1} \right) \\ &= \frac{A}{\pi} \lim_{\varepsilon \rightarrow 0} \text{Re} \int_{-\frac{\Lambda\beta}{2a} + i\varepsilon}^{\infty + i\varepsilon} d\omega \frac{\omega^2 - 1 + \kappa^2/2 + \tilde{S}^2/2}{\sqrt{(\omega^2 - 1 + \kappa^2)(\omega^2 - 1)}} \frac{1}{e^{\beta(A\omega - \mu)} + 1} \\ &= \frac{\mu}{\pi} - \frac{A}{\pi^2} \int_0^{\pi/2} d\varphi \left(\Delta_\varphi + \frac{\tilde{S}^2 - 2 + \kappa^2}{2\Delta_\varphi} \right) \text{Re} \left[\psi \left(\frac{1}{2} + \frac{i\beta}{2\pi}(\mu + A\Delta_\varphi) \right) - (A \rightarrow -A) \right]. \end{aligned} \quad (42)$$

With Eqs. (24) and (37) we readily check that its spatial average satisfies $\langle \rho(x) \rangle = -\partial\Psi/\partial\mu$. We will evaluate $\rho(x)$ analytically at $T = 0$ in the following section.

4 Phase boundaries, zero temperature limit and multicritical point

Limit $\kappa \rightarrow 0$, perturbative phase boundary

Here we are interested in the boundary between the chirally restored phase and the crystal. In Ref. [19] it has already been determined via almost degenerate perturbation theory. As a cross-check we rederive it from the full thermodynamic potential. A straightforward expansion of F_2 [use Eq. (39)] yields

$$F_2 = -\frac{a\kappa^4}{32} \frac{\partial}{\partial a} \text{Re} \left[\psi \left(\frac{1}{2} + \frac{i}{2\pi}(\nu + a) \right) + (a \rightarrow -a) \right] + \mathcal{O}(\kappa^6). \quad (43)$$

With Eq. (38) we can summarize the equations for the $\kappa \rightarrow 0$ phase boundary by

$$\ln \frac{1}{4\pi T} = \frac{1}{2} \min_{a \geq 0} \text{Re} \left[\psi \left(\frac{1}{2} + \frac{i}{2\pi}(\nu + a) \right) + (a \rightarrow -a) \right]. \quad (44)$$

The resulting curve is included in Figs. 5 and 6 (label “ $\kappa = 0$ ”). For small ν where $\text{Re} \left[\psi \left(2, \frac{1}{2} + \frac{i\nu}{2\pi} \right) \right] < 0$ ($\psi(2, x) = d^2\psi(x)/dx^2$ etc.), the unique minimum is at $a = 0$. In this range of ν the phase boundary does not touch the crystal region in the (μ, T) -diagram. It corresponds to the transition between the massless and the massive homogeneous solutions described by

$$\ln \frac{1}{4\pi T} = \text{Re} \psi \left(\frac{1}{2} + \frac{i\nu}{2\pi} \right). \quad (45)$$

The critical temperature at $\mu = 0$ (using $\psi(1/2) = -C - \ln 4$) coincides with the known value

$$T_c = \frac{e^C}{\pi}. \quad (46)$$

The tricritical point is situated at ν_t with

$$\text{Re} \psi \left(2, \frac{1}{2} + \frac{i\nu_t}{2\pi} \right) = 0, \quad \nu_t = 1.910668 \quad (47)$$

One finds $\mu_t = 0.608221$, $T_t = 0.318329$, $\beta_t = 3.141401$ in agreement with the tricritical point of the old phase diagram [11].

For $\nu > \nu_t$ the right hand side of Eq. (44) develops a minimum for $a > 0$, whereas $a = 0$ becomes a maximum (implying $T(a > 0) > T(a = 0)$). Here Eq. (44) defines the boundary between the massless homogeneous and the crystal phase. In the neighbourhood of this boundary a leading order expansion allows us to analytically compare the values of the minimized potential density in the crystal phase with the massless homogeneous potential $\Psi(\kappa = 0) = -\pi/6\beta^2 - \mu^2/2\pi$. To this end we fix a $\nu = \mu/T = \text{const.}$ line in the (μ, T) -diagram. This line has a unique intersection point $P_0 = (\mu_0, T_0)$ with the phase boundary. The value a_0 of a at P_0 is determined by the location of the minimum in Eq. (44). Now we determine the minimum value of Ψ_{ren} on the $\nu = \text{const.}$ line in the neighbourhood of P_0 as a function of T (and ν, a_0, T_0) and compare it with the $\kappa = 0$ result. We obtain

$$\Psi_{\text{ren, min}} = \Psi_{\text{ren, } \kappa=0} + \frac{16\pi(T - T_0)^2}{\text{Re} \left[\psi \left(2, \frac{1}{2} + \frac{i}{2\pi}(\nu + a_0) \right) + (a_0 \rightarrow -a_0) \right]}. \quad (48)$$

The minimum condition in Eq. (44) implies $0 < d^2(\text{r.h.s.})/da^2$ at $a = a_0$ and thus $\Psi_{\text{ren},\min} < \Psi_{\text{ren},\kappa=0}$ for $T < T_0$, $\nu > \nu_t$. The crystal solution is thermodynamically favorable. This proves that a phase transition occurs. The $(T - T_0)$ -dependence shows that it is of second order.

Limit $\kappa \rightarrow 1$, non-perturbative phase boundary

This limit is relevant for the phase transition between crystal and massive phases as well as for the translationally unbroken, chirally broken “massive” phase alone.

The relation between a and ν along the (non-perturbative) phase boundary is determined by $F_2 = 0$ or equivalently

$$\frac{1}{4a} \lim_{\kappa \rightarrow 1} \ln(1 - \kappa^2) F_2(\kappa) = \frac{\partial}{\partial a} \frac{1}{a} \int_0^{\pi/2} d\varphi \frac{1}{\cos \varphi} \text{Im} \ln \frac{\Gamma\left(\frac{1}{2} + \frac{i}{2\pi}(\nu + a \cos \varphi)\right)}{\Gamma\left(\frac{1}{2} + \frac{i}{2\pi}(\nu - a \cos \varphi)\right)} = 0. \quad (49)$$

With these values for a and ν

$$F_1(\kappa = 1) = -\ln \frac{\beta}{4\pi} + \frac{1}{\pi} \int_0^\pi d\varphi \text{Re} \psi\left(\frac{1}{2} + \frac{i}{2\pi}(\nu + a \cos \varphi)\right) = 0 \quad (50)$$

determines β at the phase boundary. The resulting curve is shown in the phase diagram in Fig. 5 (label “ $\kappa = 1$ ”). An expanded plot which reveals more details about the shape of the curve is displayed in Fig. 6. Eq. (50) alone with values of (a, ν) that are not restricted by Eq. (49) gives the connection between a , ν and β in the massive phase away from the crystal region.

As in the case $\kappa \rightarrow 0$ we can perform an analytical near-boundary comparison between the crystal and the massive phase. The result is

$$\Psi_{\text{ren},\min} = \Psi_{\text{ren},\kappa=1} + \frac{2a_0^2 T_0}{\pi} \frac{T - T_0}{\ln(T - T_0)} \quad (51)$$

where the relation between a_0 and ν is given by Eq. (49). Since $T > T_0$, $\ln(T - T_0) < 0$ in the crystal phase near the phase boundary, we have again established that the phase transition is genuine: In the region where mathematically both phases exist, the crystal phase has lower potential. The $(T - T_0)$ -dependence again shows that the transition is second order.

Limit $T \rightarrow 0$

Many equations simplify remarkably in the limit $T \rightarrow 0$, although the ansatz for $S(x)$ is basically unaltered. The solution of the $T = 0$ case has been presented before [22]. Here we want to show how to regain the $T = 0$ results from the general setting.

We start from Eqs. (38), (39) and (40) where we use asymptotic relations for large z : $\text{Im} \ln \Gamma(1/2 + iz) \sim z(\ln |z| - 1)$, $\text{Re} \psi(1/2 + iz) \sim \ln |z|$ (here, $z = \beta(\mu \pm A\Delta_\varphi)/2\pi$). The integrals are best evaluated for $\mu > A$, where we do not have to account for the absolute value in the logarithms. The general result is recovered by taking the (unique) real value of the multivalued analytic continuation to $\mu < A$. Standard techniques (e.g. substitute

$\Delta_\varphi = x$ and transform the integrals into contour integrals in the complex plane) yield

$$\begin{aligned}
F_{1,\text{ren}}(T=0) &= \text{Re} \ln \left(\sqrt{\mu^2 - A^2 + A^2\kappa^2} + \sqrt{\mu^2 - A^2} \right) \\
F_2(T=0) &= -\frac{\mathbf{E}}{\mathbf{K}} - \text{Re} \frac{\mu}{A} \left[\left(1 - \frac{\mathbf{E}}{\mathbf{K}}\right) \mathbf{F} \left(\frac{A}{\mu}, \sqrt{1 - \kappa^2} \right) - \mathbf{E} \left(\frac{A}{\mu}, \sqrt{1 - \kappa^2} \right) \right] \\
\Psi_1(T=0) &= -\frac{\mu^2}{2\pi} + \frac{1}{4\pi} \text{Re} \left[\sqrt{\mu^2 - A^2 + A^2\kappa^2} - \sqrt{\mu^2 - A^2} \right]^2
\end{aligned} \tag{52}$$

where $\mathbf{F}/\mathbf{E}(x, \kappa) = \int_0^x (1-t^2)^{-1/2} (1-\kappa^2 t^2)^{\mp 1/2}$ are the incomplete elliptic integrals of the first and second kind. For positive A the only solution of $F_{1,\text{ren}} = F_2 = 0$ falls into the range $A^2(1 - \kappa^2) < \mu^2 < A^2$ where Eqs. (52) simplify to (use $\mathbf{E}\mathbf{K}' + \mathbf{E}'\mathbf{K} - \mathbf{K}\mathbf{K}' = \pi/2$)

$$\begin{aligned}
F_{1,\text{ren}}(T=0) &= \ln(A\kappa) \\
F_2(T=0) &= -\frac{\mathbf{E}}{\mathbf{K}} + \frac{\mu}{A} \frac{\pi}{2\mathbf{K}} \\
\Psi_1(T=0) &= \frac{A^2\kappa^2}{4\pi} - \frac{A^2}{2\pi}.
\end{aligned} \tag{53}$$

Solving $F_{1,\text{ren}} = F_2 = 0$ gives

$$A = \frac{1}{\kappa} \tag{54}$$

and the following parameter representation of the grand canonical potential density,

$$\Psi_{\text{ren}} = \frac{1}{4\pi} - \frac{1}{2\pi\kappa^2}, \quad \mu = \frac{2\mathbf{E}}{\pi\kappa}. \tag{55}$$

We confirm that $A^2(1 - \kappa^2) < \mu^2 < A^2$ and find that $\Psi_{\text{ren}} < \Psi_{\text{ren}}(\kappa = 1)$ and $\Psi_{\text{ren}} < \Psi_{\text{ren}}(A = 0) = -\mu^2/2\pi$. (For large μ we have $\Psi_{\text{ren}} = -\mu^2/2\pi - \mu^{-2}/64\pi$.) This is consistent with the phase transition at $\mu = \mu(\kappa = 1) = 2/\pi$.

Moreover

$$\begin{aligned}
\rho(T=0) &= -\frac{\partial}{\partial\mu}\psi = \frac{1}{2\kappa\mathbf{K}} \quad \text{and} \\
E_{\text{ren}}(T=0) &= \Psi_{\text{ren}} + \mu\rho = \frac{1}{4\pi} + \frac{1}{\pi\kappa^2} \left(\frac{\mathbf{E}}{\mathbf{K}} - \frac{1}{2} \right).
\end{aligned} \tag{56}$$

We recover the value of the Fermi momentum $p_{\text{F}} = \pi\rho$ at $T = 0$ from Ref. [22].

In Figs. 7 and 8, Ψ_{ren} is plotted together with the self-consistent solution of the homogeneous phases (two curves for the ‘‘massive’’ phase corresponding to the minimum and maximum of Ψ_{ren} and one curve for the ‘‘massless’’ phase).

We end this section with a $T = 0$ analysis of the x -dependent baryon density. From Eq. (42) we obtain

$$\rho(x, T=0) = \frac{1}{2\kappa\mathbf{K}} - \frac{\mathbf{K}'}{2\pi\kappa} \left(\tilde{S}^2(x/\kappa) - s^2 \right). \tag{57}$$

This expression has the following high and low-density limits: At low density ($\kappa \rightarrow 1$) we recover the result for a single baryon

$$\rho(x, T = 0, \kappa \rightarrow 1) \approx \frac{1}{4 \cosh^2 x} + \frac{1}{4 \cosh^2(x/\kappa + \mathbf{K})}. \quad (58)$$

At high density ($\kappa \rightarrow 0$) the total baryon density is constant

$$\rho(x, T = 0, \kappa \rightarrow 0) \approx \frac{1}{2\kappa\mathbf{K}}. \quad (59)$$

Limit $a \rightarrow 0$, perturbative phase boundary and tricritical point

For all prominent functions in this paper the power series at $a = 0$ can be given in closed form. With c_n defined by

$$\frac{\omega^2}{\sqrt{(\omega^2 - 1 + \kappa^2)(\omega^2 - 1)}} = \sum_{n=0}^{\infty} c_n \omega^{-2n} \quad (60)$$

we find $c_0 = 1$, $c_1 = 1 - \kappa^2/2$, $c_2 = 1 - \kappa^2 + 3\kappa^4/8$ and in general

$$c_n = \frac{2}{\pi} \int_0^{\pi/2} d\varphi \Delta_{\varphi}^{2n} = \sum_{k=0}^n \binom{2k}{k} \binom{n}{k} \left(-\frac{\kappa^2}{4}\right)^k. \quad (61)$$

We obtain

$$\begin{aligned} F_{1,\text{ren}} &= -\ln \frac{\beta}{4\pi} + \sum_{n=0}^{\infty} \left(-\frac{a^2}{4\pi^2}\right)^n \frac{c_n}{(2n)!} \text{Re} \psi \left(2n, \frac{1}{2} + \frac{i\nu}{2\pi}\right) \\ F_2 &= \sum_{n=1}^{\infty} \left(-\frac{a^2}{4\pi^2}\right)^n \frac{((1 - \kappa^2)c_{n-1} - \frac{\mathbf{E}}{\mathbf{K}}c_n)}{(2n-1)!(2n+1)} \text{Re} \psi \left(2n, \frac{1}{2} + \frac{i\nu}{2\pi}\right) \\ \pi\beta^2\Psi_{\text{ren}} &= -\frac{\pi^2}{6} - \frac{\nu^2}{2} + a^2 \sum_{n=0}^{\infty} \left(-\frac{a^2}{4\pi^2}\right)^n \frac{c_{n+1} - \frac{\mathbf{E}}{\mathbf{K}}c_n}{(2n+1)!} \left[\text{Re} \psi \left(2n, \frac{1}{2} + \frac{i\nu}{2\pi}\right) - \delta_{n,0} \ln \frac{\beta}{4\pi} \right]. \end{aligned} \quad (62)$$

In the following we want to study the tricritical point by expanding the thermodynamical potential density to order a^6 . The result from minimizing Ψ_{ren} with respect to a and κ is encoded in the fourth order expansions of $F_{1,\text{ren}} = F_2 = 0$. From $F_2 = 0$ we find

$$\frac{a^2}{4\pi^2} = 10 G_1(\kappa^2) \frac{\text{Re} \psi(2, \frac{1}{2} + \frac{i\nu}{2\pi})}{\text{Re} \psi(4, \frac{1}{2} + \frac{i\nu}{2\pi})} \quad (63)$$

with

$$G_1(\kappa^2) = \frac{(1 - \kappa^2)c_0 - \frac{\mathbf{E}}{\mathbf{K}}c_1}{(1 - \kappa^2)c_1 - \frac{\mathbf{E}}{\mathbf{K}}c_2} \quad (64)$$

and the limits

$$G_1(0) = \frac{3}{5}, \quad G_1(1) = \frac{4}{3}. \quad (65)$$

If the right hand side of Eq. (63) is positive, there exists a non-trivial solution for a . The equation $F_1 = 0$ determines β as function of κ and ν to

$$\ln \frac{\beta}{4\pi} = \operatorname{Re} \psi \left(\frac{1}{2} + \frac{i\nu}{2\pi} \right) - \frac{5}{6} G_2(\kappa^2) \frac{\left[\operatorname{Re} \psi \left(2, \frac{1}{2} + \frac{i\nu}{2\pi} \right) \right]^2}{\operatorname{Re} \psi \left(4, \frac{1}{2} + \frac{i\nu}{2\pi} \right)} \quad (66)$$

with

$$G_2(\kappa^2) = G_1(\kappa^2) \frac{(1 - \kappa^2)(1 - \kappa^2 - \frac{3}{8}\kappa^4) - \frac{\mathbf{E}}{\mathbf{K}} c_1 c_2}{(1 - \kappa^2)c_1 - \frac{\mathbf{E}}{\mathbf{K}} c_2} \quad (67)$$

and the limits

$$G_2(0) = \frac{9}{5}, \quad G_2(1) = \frac{2}{3}. \quad (68)$$

The potential density as function of κ and ν is given by

$$\pi\beta^2\Psi_{\text{ren}} = -\frac{\pi^2}{6} - \frac{\nu^2}{2} - \frac{50\pi^2\kappa^4}{3} G_1^2(\kappa^2) \frac{(1 - \kappa^2)c_1 - \frac{\mathbf{E}}{\mathbf{K}}(1 - \kappa^2 + \frac{\kappa^4}{16})}{(1 - \kappa^2)c_1 - \frac{\mathbf{E}}{\mathbf{K}}c_2} \frac{\left[\operatorname{Re} \psi \left(2, \frac{1}{2} + \frac{i\nu}{2\pi} \right) \right]^3}{\left[\operatorname{Re} \psi \left(4, \frac{1}{2} + \frac{i\nu}{2\pi} \right) \right]^2}. \quad (69)$$

The two phase boundaries of the crystal phase correspond to $\kappa = 0, 1$. By using Eqs. (66) and (67), one can plot $T = 1/\beta$ against $\mu = \nu/\beta$ for $\nu \geq \nu_t$ and construct these phase boundaries near the Lifshitz point. The third, ‘‘old’’ phase boundary follows similarly from Eq. (45) for $\nu \leq \nu_t$. Finally, in the vicinity of the Lifshitz point, we can expand (T, μ) around (T_t, μ_t) and derive the (approximate) phase boundaries in closed analytical form. Starting from Eq. (66), we find to second order

$$\ln \frac{\beta}{\beta_t} = -A_1(\nu - \nu_t) - A_2(\nu - \nu_t)^2 \quad (70)$$

with

$$\begin{aligned} A_1 &= \frac{1}{2\pi} \operatorname{Im} \psi \left(1, \frac{1}{2} + \frac{i\nu_t}{2\pi} \right) \\ A_2 &= \frac{5}{24\pi^2} G_2(\kappa^2) \frac{\left[\operatorname{Im} \psi \left(3, \frac{1}{2} + \frac{i\nu_t}{2\pi} \right) \right]^2}{\operatorname{Re} \psi \left(4, \frac{1}{2} + \frac{i\nu_t}{2\pi} \right)} \end{aligned} \quad (71)$$

The equation for lines of constant κ then reads

$$T - T_t = \frac{A_1 T_t}{\mu_t A_1 + T_t} (\mu - \mu_t) - \frac{(A_1^2 - 2A_2) T_t^2}{2(\mu_t A_1 + T_t)^3} (\mu - \mu_t)^2. \quad (72)$$

The linear term is independent of κ , so that all curves enter the Lifshitz point with the same slope. The quadratic term describes the κ -dependence of the curvature and changes sign as a function of κ . The limiting cases $\kappa = 0, 1$ yield the approximate phase boundaries in closed form. Furthermore, Eq. (63) shows that a^2 is linear in $\nu - \nu_t$. This translates into the behavior

$$A \sim (\mu - \mu_t)^{1/2} \quad (73)$$

along the phase boundaries and the corresponding critical exponent $1/2$ as expected by mean field theory.

Finally, we derive a Ginzburg-Landau type effective action near the Lifshitz point from the Taylor expansion of the grand canonical potential in powers of κ . For this purpose, we compute spatial averages of powers of S and its derivatives (keeping all even terms up to order A^6). Upon comparing the (analytical) results of such a calculation with Eqs. (61), we find the simple relations

$$\begin{aligned} c_1 - \frac{\mathbf{E}}{\mathbf{K}}c_0 &= \frac{s^2}{2} = \frac{1}{2A^2}\langle S^2 \rangle \\ c_2 - \frac{\mathbf{E}}{\mathbf{K}}c_1 &= \frac{3}{8A^4} \left(\langle S^4 \rangle + \langle (S')^2 \rangle \right) \\ c_3 - \frac{\mathbf{E}}{\mathbf{K}}c_2 &= \frac{5}{16A^6} \left(\langle S^6 \rangle + \frac{1}{2}\langle (S'')^2 \rangle + 5\langle S^2(S')^2 \rangle \right) \end{aligned} \quad (74)$$

This enables us to write down a Ginzburg-Landau effective action as follows,

$$\begin{aligned} \Psi_{\text{eff}} &= -\frac{\pi}{6}T^2 - \frac{\mu^2}{2\pi} + \frac{1}{2\pi}S^2 \left[\ln(4\pi T) + \text{Re} \psi \left(\frac{1}{2} + \frac{i\mu}{2\pi T} \right) \right] \\ &\quad - \frac{1}{2^6\pi^3 T^2} \left(S^4 + (S')^2 \right) \text{Re} \psi \left(2, \frac{1}{2} + \frac{i\mu}{2\pi T} \right) \\ &\quad + \frac{1}{2^{11}3\pi^5 T^4} \left(S^6 + \frac{1}{2}(S'')^2 + 5S^2(S')^2 \right) \text{Re} \psi \left(4, \frac{1}{2} + \frac{i\mu}{2\pi T} \right) \end{aligned} \quad (75)$$

(This result can be applied to the translationally symmetric solution by simply dropping all the derivatives of S .) At the tricritical point, both the S^2 and $S^4 + (S')^2$ terms vanish, see Eqs. (45) and (47). This is the reason why we had to include terms up to the order S^6 .

For completeness we report that we have found another self-consistent solution of the Dirac Hartree-Fock equation which corresponds to the $j = 2$ (double gap) Lamé equation. The scalar density for this solution is

$$S_{j=2}(x) = 6A\kappa^2 \frac{\text{sn}(Ax, \kappa)\text{cn}(Ax, \kappa)\text{dn}(Ax, \kappa)}{1 + \kappa^2 + \sqrt{1 - \kappa^2} + \kappa^4 - 3\kappa^2\text{sn}^2(Ax, \kappa)} \quad (76)$$

where again A and κ have to take specific values to ensure self-consistency for given μ and T . The solution was found to be analytically accessible, being just slightly more involved than the $j = 1$ case. However, the result showed that (as physically expected from the gap-structure) the solution always lies higher in grand potential than the $j = 1$ case. Moreover, in general it does not correspond to a local minimum in the space of scalar potentials, having unstable directions. Therefore we refrain from writing down explicit equations. Instead we show in Fig. 8 a closeup of the $T = 0$ plot (Fig. 7) of the grand canonical potential density with the $j = 2$ case included (in its range of existence $\frac{5}{12} < \mu^2 < \frac{3}{4}$).

5 Relation to condensed matter physics

In a previous paper, we have pointed out that GN type models can be reinterpreted as relativistic superconductors [27]. This is due to a 2-dimensional remnant of the Pauli-Gürsey symmetry of massless fermions [28, 29]. It allows us to define “particle” and “anti-particle” independently for left-handed and right-handed quarks. Models with fermion-antifermion pairing (chiral condensate) and fermion-fermion pairing (Cooper pairs) can then be mapped onto each other by a “duality” transformation. The phase diagram which we have discussed above is equivalent to the phase diagram of a theory with Lagrangian

$$\mathcal{L} = \bar{\psi}^{(i)} i \not{\partial} \psi^{(i)} + \frac{g^2}{2} \left(\psi_R^{(i)\dagger} \psi_L^{(i)\dagger} + \psi_L^{(i)} \psi_R^{(i)} \right)^2, \quad (77)$$

provided we replace the chemical potential $\mu = \mu_R + \mu_L$ by the axial chemical potential $\mu_5 = \mu_R - \mu_L$ (see Ref. [27]). The kink-antikink phase of the GN model can then be identified with the Larkin-Ovchinnikov-Fulde-Ferrel (LOFF) phase [30, 31] of the dual model. Such inhomogeneous superconductors have recently attracted considerable attention in the context of QCD (for a current review article, see Ref. [32]).

Actually, there is yet another kind of connection between the GN model and non-relativistic condensed matter systems which is even more surprising. Although the GN model is mentioned occasionally in the corresponding condensed matter literature (see e.g. [33, 34]), it seems that this close relationship has never been exploited in a systematic way. The physics of the problems we have in mind is totally different from the GN model, yet the mathematical analogies are striking. Let us discuss a few pertinent references which we came across when looking for parallels between the phase diagram of the GN model and that of quasi-one-dimensional solid state systems. This may be regarded as a continuation of the work of Jackiw and Schrieffer [35] on kinks in condensed matter and relativistic field theories to finite kink densities.

The first example is a 1981 paper by Mertsching and Fischbeck on the Peierls-Fröhlich model [36]. These authors address the quasi-one-dimensional Fröhlich model with a nearly half-filled band, an electron-phonon system. They are interested in the phase diagram, notably the transition between commensurate-incommensurate charge density waves, using a mean field approximation. There seems to be a mathematical one-to-one correspondence between this system and the GN model. The authors of Ref. [36] have also found the analytic solution to the mean field equation, guided by the Landau expansion around the triple point (which is called Leung point [37] in this context). Crucial for the close correspondence with a relativistic field theory are evidently a continuum approximation (the lattice constant acts as inverse cutoff and is taken to 0) and a linearization of the electron dispersion relation near the Fermi surface (simulating “ultrarelativistic kinematics”). In appropriate units, the results are identical to ours, as far as we can tell.

In a subsequent paper, Machida and Nakanishi [38] used the phase diagram of Ref. [36] in a different physics context: They studied the interplay of superconductivity and ferromagnetism in ErRh_4B_4 (Erbium-Rhodium-Boride). Thanks to a number of approximations (in particular the one-dimensional band model with linear dispersion) they managed to reduce this problem mathematically to the Peierls-Fröhlich model. For real order param-

eter, their results are again fully equivalent to ours for the GN model, except that now one has to use another dictionary: The Dirac equation corresponds to the Bogoliubov-deGennes equation, particle/antiparticle degrees of freedom to spin (which exists in a quasi-one-dimensional world), chemical potential to magnetic field, baryon density to spin polarization. Our three phases (massive, crystal and massless) correspond to their BCS, “sn” and normal phases, respectively. The order parameter at $T = 0$ looks different from ours at first sight. However, the two expressions can be converted into each other by Landen’s transformation for Jacobi functions [25] in the form

$$\kappa \frac{\operatorname{sn}(\xi, \kappa) \operatorname{cn}(\xi, \kappa)}{\operatorname{dn}(\xi, \kappa)} = \frac{1 - \kappa'}{\kappa} \operatorname{sn} \left((1 + \kappa') \xi, \frac{1 - \kappa'}{1 + \kappa'} \right), \quad \kappa' = \sqrt{1 - \kappa^2}. \quad (78)$$

Not only the phase boundaries, but all observables can be identified if one keeps in mind the above mentioned dictionary. Nevertheless, there are subtle differences which show that one should not take over results blindly: The authors of Ref. [38] also discuss complex order parameters, in particular a helical phase. In the discrete chiral GN model, the order parameter is always real. In the continuous chiral NJL₂ model, it can be complex and we have indeed found a helical phase [15], but the results for the phase diagram are different. Here apparently the quantitative correspondence between relativistic field theory and solid state physics ends due to some differences in dynamics.

As a third example, we would like to mention the more recent work of Buzdin and Kachkachi [39]. They derive the Ginzburg-Landau theory for nonuniform LOFF superconductors near the tricritical point in the (T, H) -phase diagram in one, two and three dimensions. If we take their result for one dimension and specialize it to a real order parameter, we find perfect agreement between our Eq. (75) and their Eq. (3) in appropriate units (a discrepancy in the sign of the $|\psi|^2$ term must be due to a misprint). We have to identify their magnetic field \mathcal{H}_0 with our chemical potential μ . One can find many more similar studies in the literature, see e.g. the recent review article on stripe phases [40].

Our fourth example is related to solitons in trans-polyacetylene, starting with the seminal paper by Su, Schrieffer and Heeger [41]. In this case there have been efforts to bridge the gap between particle and solid state physics by Chodos and Minakata [42, 43]. Since these authors start from the old phase diagram of the Gross-Neveu model, they notice that there are some discrepancies with the soliton lattice theory of Horowitz [44]. However, the analytical results of Horowitz agree perfectly with our kink-antikink crystal so that everything falls into place. Let us also mention in passing the results of Okuno and Onodera on the coexistence of a soliton and a polaron in trans-polyacetylene [45] which are apparently closely related to the recent work of Feinberg [46] on the analogous phenomenon in the Gross-Neveu model.

Finally, when browsing through the literature on superconductivity, we were amused to discover that the “old” phase diagram of the GN model (assuming unbroken translational invariance) is ubiquitous in textbooks and articles on BCS theory (see e.g. Ref. [47], Fig. 6.2). It seems to go back to a 1963 paper [48] which predates the original GN paper by more than one decade and the first published GN phase diagram by more than two decades.

Summarizing, we find it gratifying that the GN model with its simple Lagrangian gives rise to such a physically rich phase diagram. Its structure seems to be mirrored by a variety of quasi-one-dimensional condensed matter systems. With hindsight, one might ask the question why it took much longer to solve the same mathematical problem in relativistic quantum field theory than in condensed matter physics. We feel that this is due to the almost exclusive use of path integral methods in particle physics. Apparently, these methods are not yet sufficiently developed to yield non-trivial saddle points with unexpected symmetry breakdown as in the present case. By contrast, canonical mean-field calculations offer a rich spectrum of approximation methods (variational, numerical etc.) which can be successively refined and used to nail down eventually the exact solution as in the case at hand. It is probably not accidental that we arrived at the phase diagram of the GN model using Hartree-Fock methods akin to the standard tools of condensed matter physics.

References

- [1] D. J. Gross and A. Neveu, Phys. Rev. D **10**, 3235 (1974).
- [2] G. 't Hooft, Nucl. Phys. B **72**, 461 (1974).
- [3] V. Schön and M. Thies, in: *At the frontier of particle physics: Handbook of QCD*, Boris Ioffe Festschrift, ed. by M. Shifman, Vol. 3, ch. 33, p. 1945, World Scientific, Singapore (2001).
- [4] Y. Nambu and G. Jona-Lasinio, Phys. Rev. **122**, 345 (1960); *ibid.* **124**, 246 (1961).
- [5] C.G. Callan, S. Coleman, D.J. Gross, and A. Zee, unpublished (referred to by [6]).
- [6] R.F. Dashen, B. Hasslacher, and A. Neveu, Phys. Rev. D **12**, 2443 (1975).
- [7] L.L. Salcedo, S. Levit and J.W. Negele, Nucl. Phys. B **361**, 585 (1991).
- [8] F. Lenz, M. Thies, S. Levit, and K. Yazaki, Ann. Phys. (N.Y.) **208**, 1 (1991).
- [9] B.J. Harrington and A. Yildiz, Phys. Rev. D **11**, 779 (1975).
- [10] R.F. Dashen, S.K. Ma, and R. Rajaraman, Phys. Rev. D **11**, 1499 (1975).
- [11] U. Wolff, Phys. Lett. B **157**, 303 (1985).
- [12] T.F. Trembl, Phys. Rev. D **39**, 679 (1989).
- [13] A. Barducci, R. Casalbuoni, M. Modugno, G. Pettini, and R. Gatto, Phys. Rev. D **51**, 3042 (1995).
- [14] A. Chodos, R.L. Jaffe, K. Johnson, C.B. Thorn, and V.F. Weisskopf, Phys. Rev. D **9**, 3471 (1974).

- [15] V. Schön and M. Thies, Phys. Rev. D **62**, 096002 (2000).
- [16] I. Klebanov, Nucl. Phys. B **262**, 133 (1985).
- [17] K. Ohwa, Phys. Rev. D **65**, 085040 (2002).
- [18] A. Brzoska and M. Thies, Phys. Rev. D **65**, 125001 (2002).
- [19] M. Thies and K. Urlichs, Phys. Rev. D **67**, 125015 (2003).
- [20] R.M. Hornreich, M. Luban and S. Shtrikman, Phys. Rev. Lett. **35**, 1678 (1975).
- [21] A.W. Overhauser, Adv. in Phys. **27**, 343 (1978).
- [22] M. Thies, Phys. Rev. D **69**, 067703 (2004).
- [23] E. T. Whittaker and G. N. Watson, *A Course of Modern Analysis*, Cambridge U. Press (1980).
- [24] G. V. Dunne and J. Feinberg, Phys. Rev. D **57**, 1271 (1998).
- [25] M. Abramowitz and I. Stegun (Eds.), *Handbook of Mathematical Functions*, Dover, New York (1990).
- [26] H. Li, D. Kusnezov and F. Iachello, J. Phys. A: Math. Gen. **33**, 6413 (2000).
- [27] M. Thies, Phys. Rev. D **68**, 047703 (2003).
- [28] W. Pauli, Nuovo Cim. **6**, 205 (1957).
- [29] F. Gürsey, Nuovo Cim. **7**, 411 (1958).
- [30] A.I. Larkin and Yu.N. Ovchinnikov, Sov. Phys. JETP **20**, 762 (1965).
- [31] P. Fulde and R.A. Ferrell, Phys. Rev. **135**, 550 (1964).
- [32] R. Casalbuoni and G. Nardulli, hep-ph/0305069.
- [33] D.K. Campbell and A.R. Bishop, Phys. Rev. B **24**, 4859 (1981).
- [34] A. Saxena and A.R. Bishop, Phys. Rev. A **44**, R2251 (1991).
- [35] R. Jackiw and J.R. Schrieffer, Nucl. Phys. B **190** [FS3], 253 (1981).
- [36] J. Mertsching and H.J. Fischbeck, phys. stat. sol. (b) **103**, 783 (1981).
- [37] M.C. Leung, Phys. Rev. B **11**, 4272 (1975).
- [38] K. Machida and H. Nakanishi, Phys. Rev. B **30**, 122 (1984).
- [39] A.I. Buzdin and H. Kachkachi, Phys. Lett. A **225**, 341 (1997).
- [40] S.I. Mukhin and S.I. Matveenko, Int. J. Mod. Phys. B **17**, 3749 (2003).

- [41] W.P. Su, J.R. Schrieffer and A.J. Heeger, Phys. Rev. Lett. **42**, 1698 (1979).
- [42] A. Chodos and H. Minakata, Phys. Lett. A **191**, 39 (1994).
- [43] H. Minakata and A. Chodos, hep-th/9709179.
- [44] B. Horowitz, Phys. Rev. B **35**, 734 (1987).
- [45] S. Okuno and Y. Onodera, J. Phys. Soc. Jap. **52**, 3495 (1983).
- [46] J. Feinberg, Phys. Lett. B **569**, 204 (2003).
- [47] D. Saint-James, G. Sarma and E.J. Thomas, *Type II Superconductivity*, Pergamon Press (1969), p. 160.
- [48] G. Sarma, J. Phys. Chem. Solids **24**, 1029 (1963).

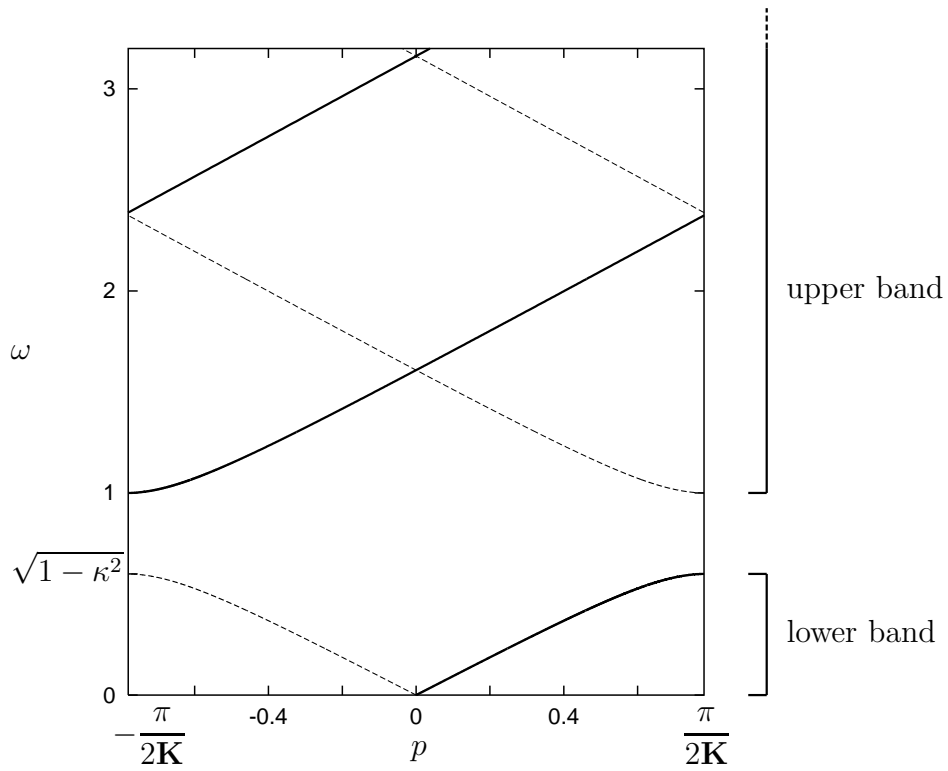


Figure 1: The dispersion relation (11) for $\kappa = 0.8$. The Bloch momentum p is projected onto the Brillouin zone ranging from $-\pi/2\mathbf{K}$ to $+\pi/2\mathbf{K}$. The bold line marks the branch for which the slope of the dispersion relation is positive. Notice the symmetry $p \rightarrow -p$.

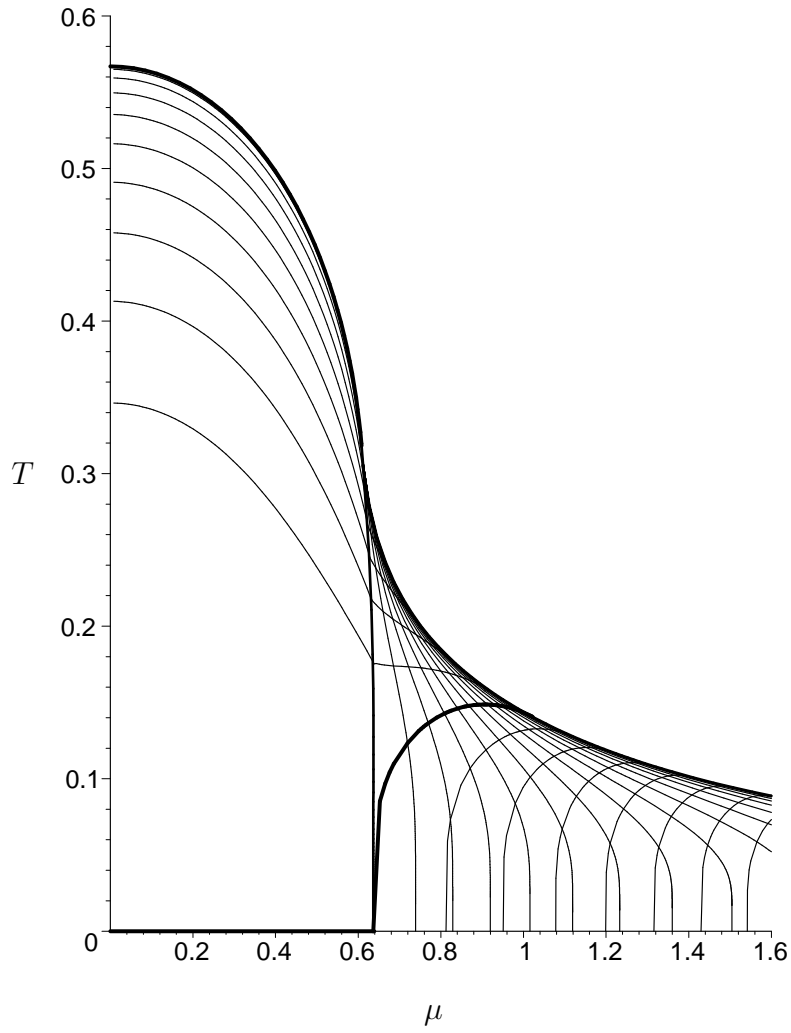


Figure 2: Lines of constant A and κ in the (μ, T) -plane, obtained by minimizing the grand potential. See Figs. 3 and 4 for more details.

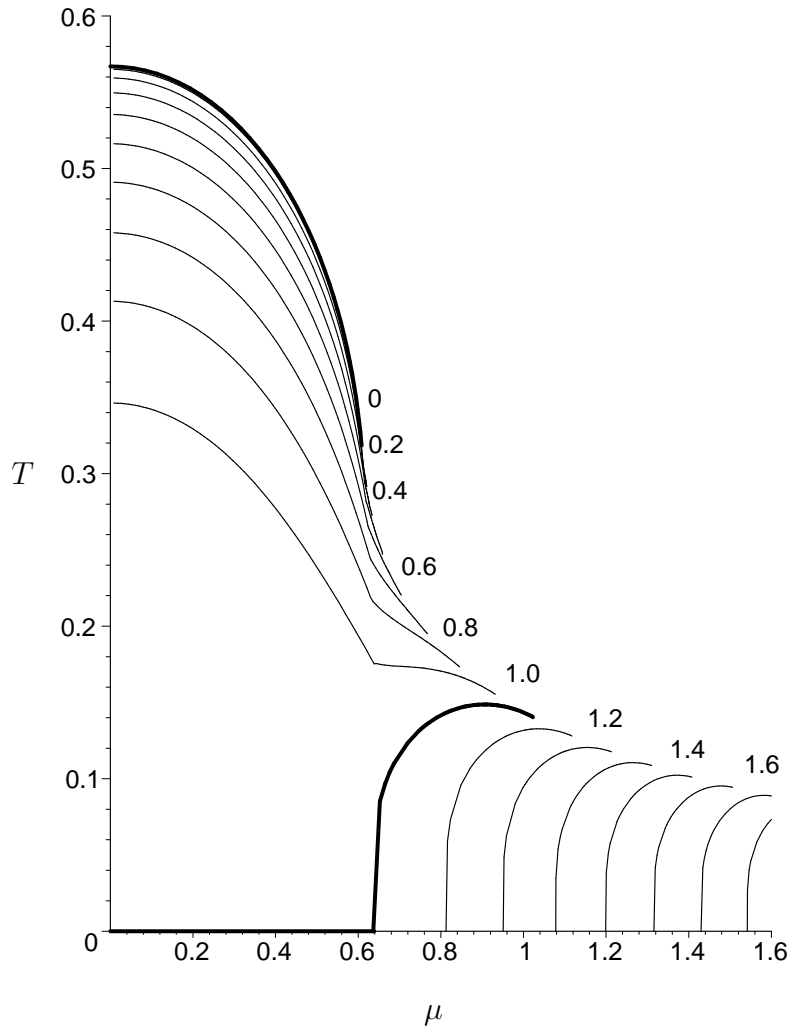


Figure 3: Contour lines $A = \text{const.}$ in the (μ, T) -plane. Thick lines: $A = 0$ and $A = 1$. A ranges from 0 to 1.7, the line spacing is $\Delta A = 0.1$.

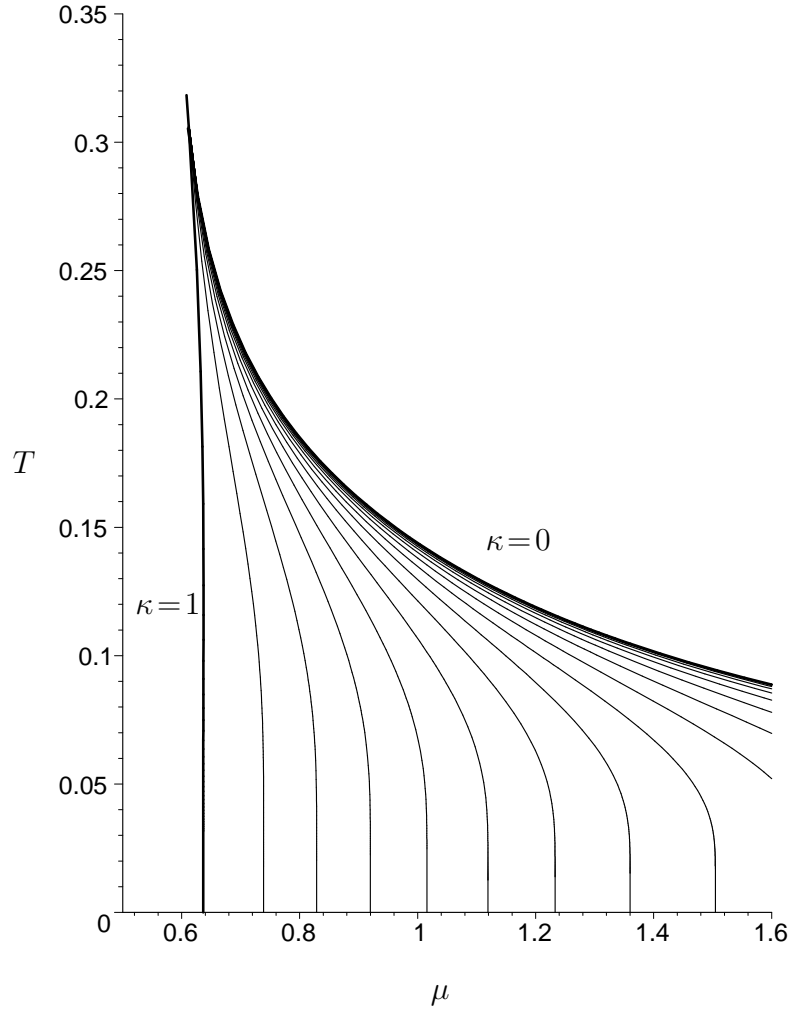


Figure 4: Contour lines $\kappa = \text{const.}$ in the crystal phase (closeup). The phase boundaries are $\kappa = 0$ and $\kappa = 1$, adjacent lines differ by $\Delta\kappa = 0.05$. All lines end at the tricritical point. At $T = 0$ we have $A\kappa = 1$ and $\mu = 2\mathbf{E}/\pi\kappa$.

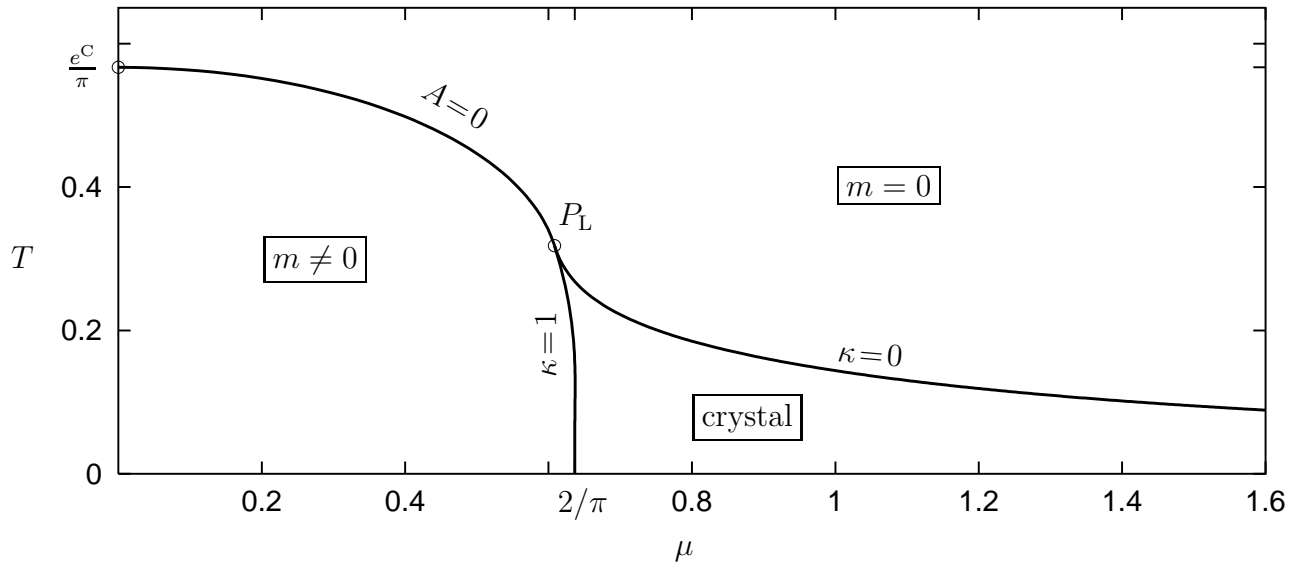


Figure 5: Phase diagram of the GN model, computed with the help of Eqs. (44), (45), (49), (50). All phase boundaries correspond to second order transitions, P_L is the Lifshitz point determined by Eqs. (45), (47).

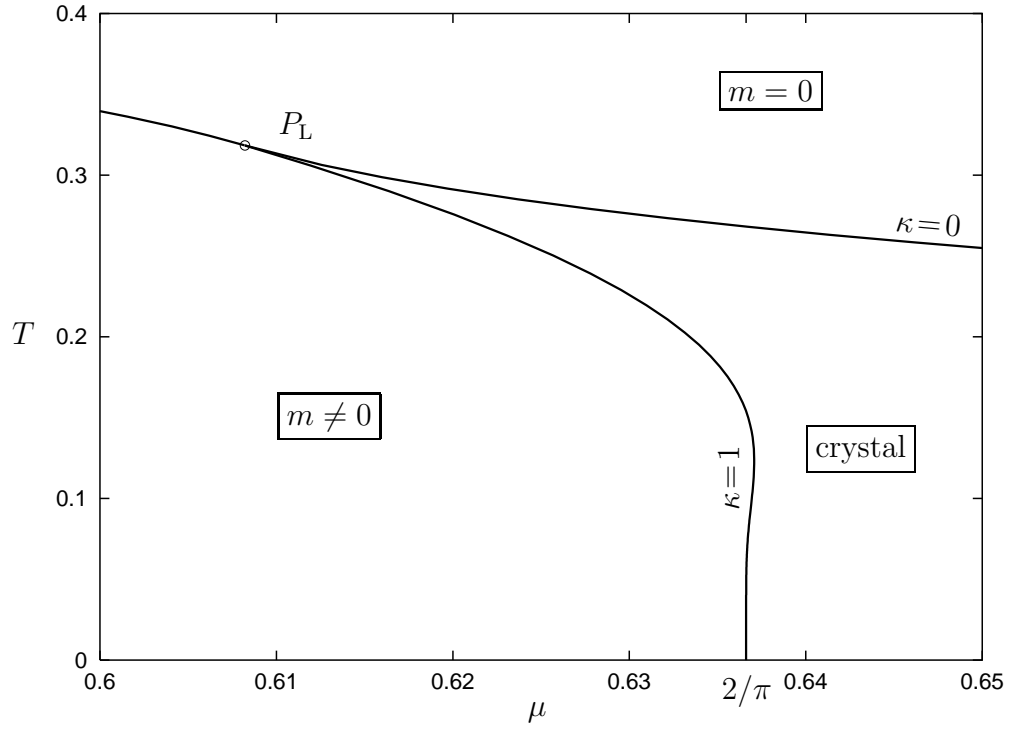


Figure 6: More detailed view of the phase boundary between homogeneous and periodic ordered phases ($\kappa = 1$). Notice the different scale on the μ -axis as compared to Fig. 5.

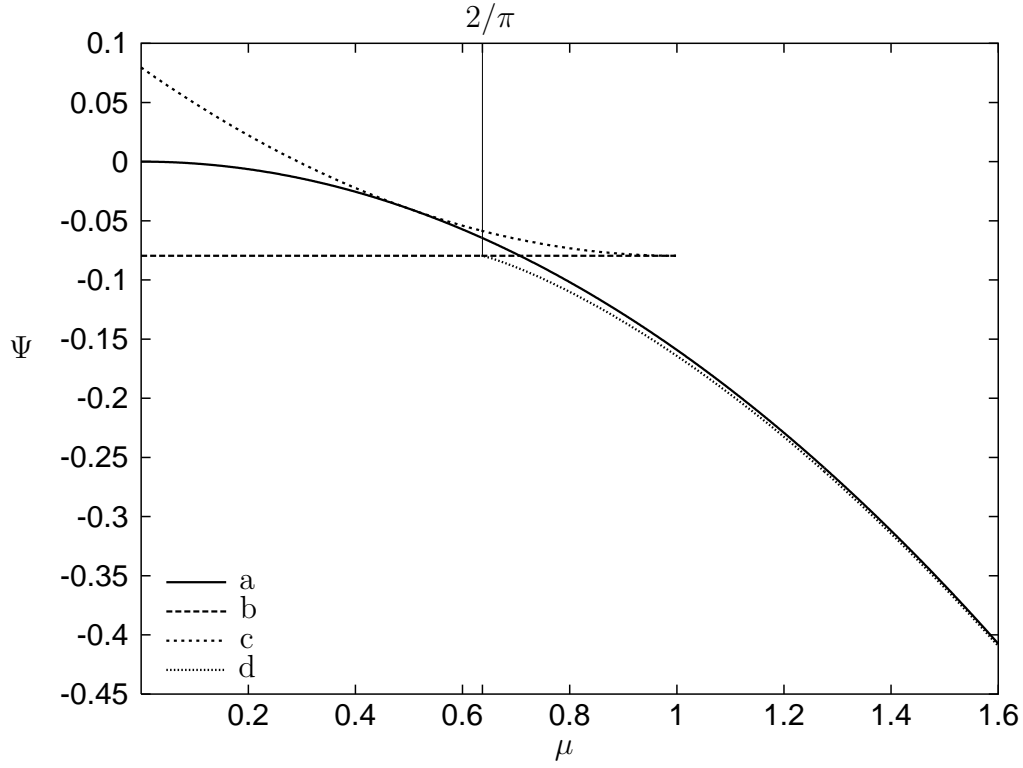


Figure 7: The grand canonical potential density Ψ for self-consistent solutions of the Dirac-Hartree-Fock equation at $T = 0$: (a) massless Fermi gas ($m = 0$), (b) and (c) the minimum and maximum solution for the massive Fermi gas ($m = 1$) and (d) the crystal solution with the Lamé potential with single gap ($j = 1$). Notice that the crystal lies below the massless Fermi gas. At $\mu = 2/\pi$, a second order phase transition between the massive Fermi gas and the crystal occurs.

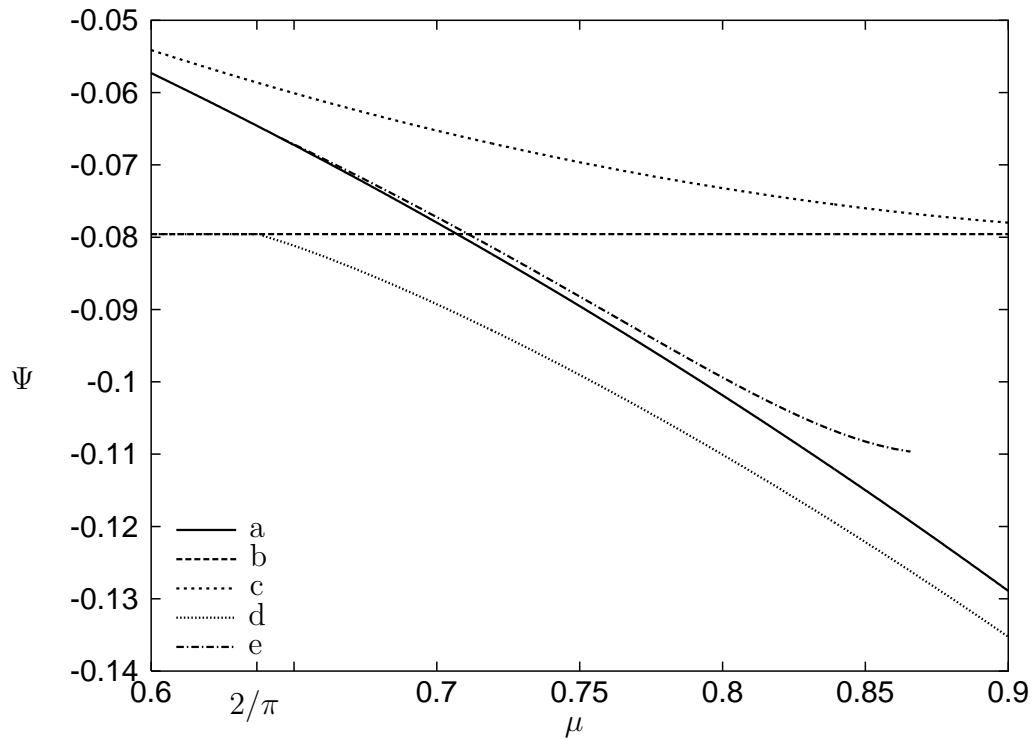


Figure 8: A closeup of Fig. 7 showing Ψ at $T = 0$ for all known self-consistent Hartree-Fock solutions. Here the (unstable) double gap Lamé solution ($j = 2$) has also been included (e).